Stroke
JOURNAL OF THE AMERICAN HEART ASSOCIATION
American Stroke Association
A Division of American Heart Association

Severe Blood-Brain Barrier Disruption and Surrounding Tissue Injury

Bo Chen, Beth Friedman, Qun Cheng, Phil Tsai, Erica Schim, David Kleinfeld and Patrick D. Lyden

Stroke published online Nov 5, 2009;
DOI: 10.1161/STROKEAHA.109.551341
Stroke is published by the American Heart Association. 7272 Greenville Avenue, Dallas, TX 72514
 Print ISSN: 0039-2499. Online ISSN: 1524-4628

Severe Blood–Brain Barrier Disruption and Surrounding Tissue Injury

Bo Chen, BS; Beth Friedman, PhD; Qun Cheng, MD; Phil Tsai, PhD; Erica Schim, MD; David Kleinfeld, PhD; Patrick D. Lyden, MD

Background and Purpose—Blood–brain barrier opening during ischemia follows a biphasic time course, may be partially reversible, and allows plasma constituents to enter brain and possibly damage cells. In contrast, severe vascular disruption after ischemia is unlikely to be reversible and allows even further extravasation of potentially harmful plasma constituents. We sought to use simple fluorescent tracers to allow wide-scale visualization of severely damaged vessels and determine whether such vascular disruption colocalized with regions of severe parenchymal injury.

Methods—Severe vascular disruption and ischemic injury was produced in adult Sprague Dawley rats by transient occlusion of the middle cerebral artery for 1, 2, 4, or 8 hours, followed by 30 minutes of reperfusion. Fluorescein isothiocyanate-dextran (2 MDa) was injected intravenously before occlusion. After perfusion-fixation, brain sections were processed for ultrastructure or fluorescence imaging. We identified early evidence of tissue damage with Fluoro-Jade staining of dying cells.

Results—With increasing ischemia duration, greater quantities of high molecular weight dextran-fluorescein isothiocyanate invaded and marked ischemic regions in a characteristic pattern, appearing first in the medial striatum, spreading to the lateral striatum, and finally involving cortex; maximal injury was seen in the mid-parietal areas, consistent with the known ischemic zone in this model. The regional distribution of the severe vascular disruption correlated with the distribution of 24-hour 2,3,5-triphenyltetrazolium chloride pallor ($r=0.75$; $P<0.05$) and the cell death marker Fluoro-Jade ($r=0.86$; $P<0.05$). Ultrastructural examination showed significantly increased areas of swollen astrocytic foot process and swollen mitochondria in regions of high compared to low leakage, and compared to contralateral homologous regions (ANOVA $P<0.01$). Dextran extravasation into the basement membrane and surrounding tissue increased significantly from 2 to 8 hours of occlusion duration (Independent samples t test, $P<0.05$).

Conclusion—Severe vascular disruption, as labeled with high-molecular-weight dextran-fluorescein isothiocyanate leakage, is associated with severe tissue injury. This marker of severe vascular disruption may be useful in further studies of the pathoanatomic mechanisms of vascular disruption-mediated tissue injury. **(*Stroke*. 2009;40:e666-e674.)**

Key Words: blood–brain barrier breakdown ■ endothelial cells ■ stroke

Pathological responses to ischemia in the microvasculature play a central role in the evolution of infarction; a critical event after ischemia is blood–brain barrier (BBB) breakdown,[1] an antecedent event to cerebral infarction and hemorrhagic transformation.[2] Increasing awareness of the interplay between vessels, glia, and neurons has led to improved understanding of the mechanisms of infarction[3] and has partially begun to explain the failures of previous neuroprotective therapies. In parallel with new understanding of the neurovascular and glial-vascular unit, preliminary data suggest direct cytotoxicity of serum constituents, such as thrombin and plasminogen,[4] in addition to the toxic effects of water entry caused by oncotic pressure shifts. The sequence of events is complex, however, because these same compounds also could occur de novo in injured parenchyma, or in the endothelium. Traditional studies of BBB leakage relied on simple measures of water flux (edema), leakage of small-molecular-weight markers (IgG or albumin labeled with Evan Blue), or very complicated and expensive ultrastructural imaging of endothelial cells, so it has been difficult to fully characterize the pathoanatomic mechanisms of injury after severe vascular disruption and to separate the effects of edema (water shift) from other putative toxic molecules. Further progress in these investigations is limited by: (1) a paucity of data regarding the time course of BBB leakage to differentially sized markers; (2) the absence of a simple, reliable marker of severe vascular disruption; and (3) quantitative measurements of leakage over time after severe

Received February 27, 2009; final revision received June 25, 2009; accepted July 24, 2009.

From Department of Neurosciences (B.C., B.F., Q.C., E.S., P.D.L.), University of California San Diego, School of Medicine, La Jolla Calif; Veterans Administration Medical Center (B.F., Q.C., P.D.L.), San Diego Calif; Department of Physics (P.T., D.K.), University of California San Diego, La Jolla Calif.

B. Chen and B. Friedman contributed equally to this work.

Correspondence to Dr Patrick Lyden, 3350 La Jolla Village Drive, San Diego, CA 92161. E-mail lydenp@cshs.org.

Stroke **is available at http://stroke.ahajournals.org** **DOI: 10.1161/STROKEAHA.109.551341**

vascular disruption. We sought to characterize severe vascular disruption with high-molecular-weight dextran-fluorescein isothiocyanate (FITC) using fluorescent, immunohistochemical, and ultrastructural confirmation, and then compared such vascular disruption to evidence of tissue injury.

Materials and Methods

All protocols were approved by the Animal Research Committee of the Veteran's Affairs Medical Center, San Diego, and by the IACUC of University of California San Diego, following all national guidelines for the care of experimental animals. The (n=71) subjects were adult male Sprague-Dawley rats (Harlan, San Diego, Calif), and average weight was 300 grams. All animals received tail-vein injections of FITC conjugated to a high-molecular-weight dextran (2 MDa; Sigma); 0.3 mL of 5% (wt/vol) solution in sterile phosphate buffered saline (PBS) at the start of surgery, eg, ≈20 minutes before occlusion of the middle cerebral artery. The subjects were allowed to awaken from anesthesia during the occlusion and reperfusion periods to allow neurological examinations with a dichotomized version of the published rodent neurological grading system.[5,6] To assure sufficient ischemia with the middle cerebral artery occlusion, only animals that registered abnormal on 3 behavioral signs were used; otherwise, the subject was excluded from further analysis. Animals were also excluded for subarachnoid hemorrhage found at postmortem dissection.

We used our version of the standard model of filament occlusion of the middle cerebral artery.[5,7] Briefly, animals were induced with isoflurane anesthesia and maintained with a mixture of 4% isoflurane in oxygen:nitrous oxide 30:70 by face mask. After adequate anesthesia and aseptic preparation, an incision was made in the neck, exposing the left common carotid artery. The external carotid and pterygopalatine arteries were ligated with 4-silk. An incision was made in the wall of the common carotid artery, which was then threaded with a 4-0 nylon suture (Ethicon) that was blunted in a microforge (Narishige MF83); filament diameters were measured using microscopy and image analysis and only filaments between 290 and 310 μm were selected for further use. The suture was advanced 17.5 mm from the bifurcation point of the external and internal carotid arteries, thereby blocking the ostium of the middle cerebral artery. At the end of the reperfusion period, the rat was euthanized with an overdose of pentobarbital and then intracardially perfused with 200 to 300 mL saline followed by 300 mL of 4% (wt/vol) paraformaldehyde in PBS.

After rapid removal from the skull, each brain was postfixed in 4% (wt/vol) paraformaldehyde in PBS and then cryoprotected in 30% sucrose to obtain 50-μm-thick sections with a freezing sliding microtome. To characterize the distribution of high-molecular-weight dextran–FITC, sequential sections through the anterior–posterior axis of the middle cerebral artery territory subsuming ≈4.5 mm of brain were sampled from ≈−0.3 bregma as an anchoring level and mounted onto glass slides. Sections were cover-slipped with Prolong Gold Antifade mountant (Molecular Probes). An additional series of sections was slide-mounted for determination of regional colocalization in the ischemic striatum of retained fluorescein with neuronal degeneration marked by Fluoro-Jade C-staining (Chemicon). Sections processed for immunocytochemistry for light microscopy incubated free-floating in antibody solutions and endogenous peroxidase was quenched with a 10-minute incubation in 3% (v/v) hydrogen peroxide in PBS. Primary antibody (anti-universal IgG; Vector) was diluted in a blocking diluent (PBS with 10% [v/v] blocking serum and 0.2% [v/v]; Triton X-100) was applied for 2 days and was followed by incubation for 4 hours in biotinylated antirabbit secondary antibody diluted in blocking diluent. Biotinylated secondary antibody was visualized by overnight incubation of sections in Cy5-conjugated streptavidin (Jackson Immunoresearch). Fluorescent immunostained sections were mounted on slides and cover-slipped with Pro-Long Antifade mountant (Molecular Probes). Background staining was assessed in sections processed without primary antibody. For ultrastructural localization of high-molecular-weight dextran–FITC after stroke, animals were prepared for transcardial perfusion–fixation and perfused with Ringer solution, followed by 4% paraformaldehyde and 0.1% glutaraldehyde in PBS solution. Brains were removed from the skull, fixed in 4% buffered paraformaldehyde overnight, and cut into 100-um thick slices on a Leica VT1000S microtome. Bound fluorescein was visualized by incubation of sections with biotinylated antifluorescein antibody (BA-0601; Vector; 1:1000 dilution) for 1 day followed by peroxidase catalysis of diaminobenzidine reporter (ABC kit PK6100 Vector and diaminobenzidine kit, SK4100; Vector). Immunostained brain slices were postfixed in 2.5% glutaraldehyde for 15 minutes on ice and then 1% osmium tetroxide for 1 hour, dehydrated, embedded in Durcupan, sectioned at 50 nM on a Reichert-Jung Ultracut E system, and mounted on coated copper grids.

Fluorescence from retained high-molecular-weight dextran–FITC was quantified within the hemisphere by semiautomated image analysis. Digitized images of the ischemic half of the brain were taken with a Zeiss microscope outfitted with CCD camera (KAF32MB; Apogee). Images were obtained at 500-μm intervals across the anterior-to-posterior axis of the middle cerebral artery territory. Fluorescence was quantified using Image Pro Plus (Cybermedia). An operator without knowledge of the subject's group or occlusion duration examined each section after first setting the magnification and performing a linear calibration using a scale bar. The operator then examined each section and set the brightness and contrast levels to optimize the appearance of the fluorescence. Using semiautomated thresholding, segmentation, and size filtering, the operator measured the total area of fluorescence. Total fluorescence typically consisted of multiple discrete "islands" on each section, and within each island there were pale areas of extravasated label intermixed with areas of very bright vascular labeling. Using an image of the islands as an overlay, the operator then re-thresholded to emphasize the bright objects contained within the islands of total fluorescence, ie, labeled vessels, and, again using segmentation and size filtering, the area of all bright vessels was measured. The area of extravasation was obtained by subtracting the area of bright fluorescence in the vessels from the total area fluorescence.

To quantify the presence of multiple fluorescent markers on single sections, we adapted a laser-scanning technique. Image acquisition was performed on an Olympus BX50 Microscope retrofitted with a CompuCyte laser scanning cytometry acquisition system. Tissue was illuminated with a focused argon laser (488 nm), and fluorescein fluorescence was collected through an emission filter of 530±30 nm. Cy5 fluorescence was illuminated with a focused helium–neon laser (633 nm), and fluorescence was collected through an emission filter bandwidth of 675±50 nm. The fluorescence was averaged over 20-μm-diameter bins (scanned areas) that encompassed the entire tissue section. Histograms were constructed to plot the regions of interest or "counts" as a function of integrated fluorescence intensity in those areas.

Background was determined by scanning subareas on the nonoccluded side of the section to obtain a histogram of the distribution of background signals. We conservatively determined a threshold for "signal" according to the maximum level of tissue background. Data were expressed as the number of scanned areas detected above background fluorescence intensities, divided by the total number of scanned areas/section. In cases with fluorescent immunostaining, similar routines were imposed to quantify immunostained regions of interest in register with fluorescein–dextran retention sites. The percent of counts with double fluorescent signals (fluorescein and Cy5) was determined from scattergram plots that were divided into 4 quadrants using Wincyte software (CompuCyte Corp).

Two-photon laser scanning microscopy was used to scan and reconstruct labeled vessels and extravasated fluorescent markers. Stacks of optically sectioned images were acquired with a 2-photon laser scanning microscope of custom design[8] using the MPScope software.[9] We used a 40×, 0.8-NA water dipping objective (IR Achroplan; Carl Zeiss Inc), 0.4 μm per pixel lateral sampling, and 0.5 μm per plane axial sampling. FITC–dextran was excited at 800

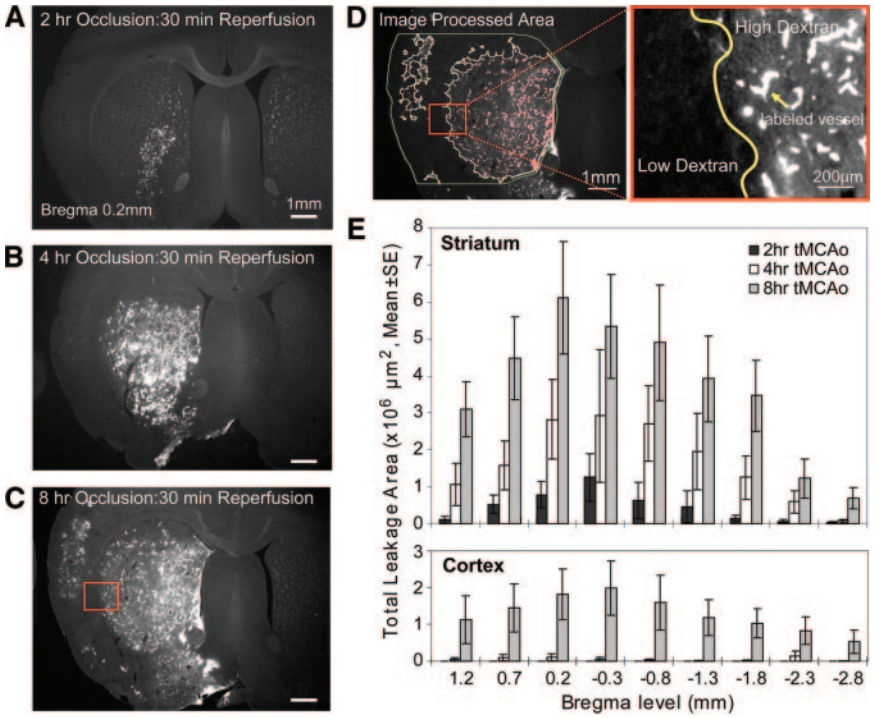

Figure 1. Severe vascular disruption after ischemic injury. Transient middle cerebral artery occlusion using a nylon filament at 2 hours (n=9), 4 hours (n=9), or 8 hours (n=6), was followed by 30 minutes of recirculation after filament removal. High-molecular-weight dextran–FITC fluorescence was measured by thresholding and semiautomated quantitation of 50-μm coronal sections obtained in the mid-parietal cortex. A, Two-hour transient middle cerebral artery occlusion and 30 minutes of reperfusion caused accumulation of the high-molecular-weight dextran in medial striatum, ipsilateral to the middle cerebral artery occlusion. B, Occlusion for 4 hours caused greater retention of the label, subsuming lateral striatum. C, The 8-hour occlusion resulted in involvement of the entire striatum and isolated areas in the cortex. The section shown in (C) is shown again in (D) after semiautomated processing, including thresholding, segmentation, and object delineation in the areas of fluorescence that could be quantified. Next to the processed view in (D), a higher magnification view of the area marked by the red box demonstrates fluorescence retention in the vessels and extravasation into parenchyma. E, Consecutive coronal levels separated by 500 μm were selected from anterior to posterior and quantified. With increasing duration of ischemia, there was a progressive accumulation of high-molecular-weight dextran–FITC in the striatum and cortex supplied by the middle cerebral artery (overall 1-way ANOVA for time, $P<0.0001$). Note the delay in accumulation in the cortex relative to striatum.

nm and the fluorescence was detected by low-pass filtering of the emission light <700 nm. Image rotation and projection operations were performed with the ImageJ software program. (NIH).

Blocks for plastic embedding were selected, based on the immunostaining for high-molecular-weight dextran–FITC, and categorized as originating from a region of high or low leakage. Blocks were also selected from homologous regions in the contralateral hemisphere. After processing as described, images were taken at 5000× on a JEOL 1200EX microscope. An examiner blind to the region of origin for each image then placed a 6×6 grid (with an interval of 2 μm between grids) on the images centered on a vessel. Using standard stereological technique,[10] the grid crossings that hit the swollen astrocytic food processes or structureless space were counted as points of "swollen cells." For the points aligning on the boundary of grids, only those on the right and bottom were counted. To normalize the results, the points that corresponded to an area of endothelial cells (including lumen space) were counted as well. Enlarged abnormal mitochondria were counted separately in each field of view. The point counts were summarized and normalized to the containing space, standardized to the calibrated grid.

Results

Vascular Disruption After Transient Middle Cerebral Artery Occlusion

Transient middle cerebral artery occlusion caused uptake of circulating high-molecular-weight dextran–FITC into vessels and extravasation into parenchyma as shown in Figure 1. The rest of the tissue section was not fluorescent because the saline perfusion removed intravascular dextran–FITC at euthanization.[11] At longer occlusion times, the subregional distribution of fluorescence expanded to include the more lateral aspect of the striatum (Figure 1B). Islands of leakage appeared in the cortex after 8 hours of middle cerebral artery occlusion (Figure 1C). Image analysis identified regions showing both labeling of the vessel walls as well as parenchymal extravasation (Figure 1D). With increasing occlusion duration, vascular damage increased in the regions supplied by the middle cerebral artery, as indicated by a significant increase in the accumulated dextran–FITC (Figure 1E).

Localization of Vascular Pathology to Regions of Severe Vascular Disruption

To demonstrate that the extravasated fluorescence seen in Figure 1 was truly extravascular, we used 2-photon imaging to optically section and reconstruct a labeled vessel and adjacent leakage (Figure 2). Epifluorescence microscopy demonstrates a swath of intensely fluorescent vessel segments (Figure 2A) on the ischemic side of the brain. In a subset of labeled vessels, a hazy fluorescence also appeared to extend into the neighboring parenchyma (Figure 2B). In the 2-photon maximal projections (Figure 2C, 2D), the intense vascular fluorescence was associated with the vessel

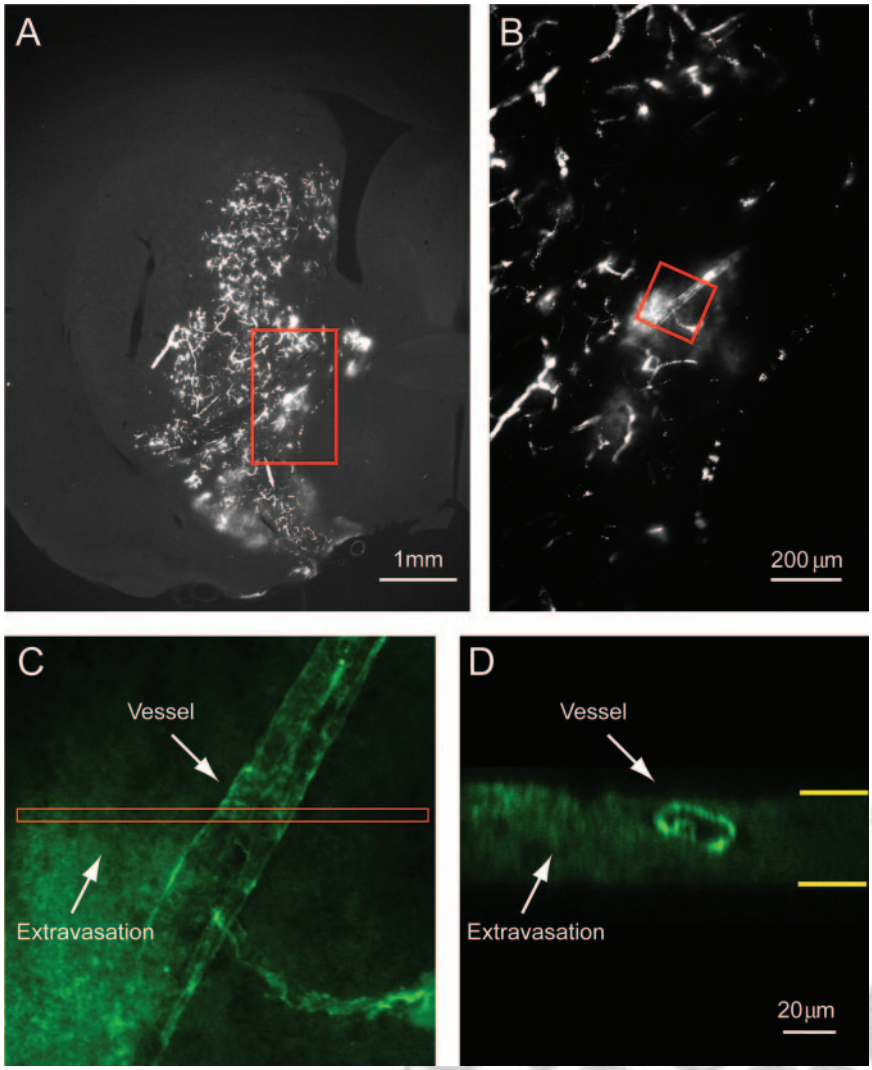

Figure 2. High-molecular-weight dextran–FITC localizes to the vessel wall and extravasates. Extravasation of high-molecular-weight dextran–FITC was measured in the regions of brain subjected to severe ischemia. A, Epi-fluorescent image of a section from a rat with 4-hour middle cerebral artery occlusion shows vascular labeling and extravasation as in Figure 1. B, Photomicrograph of vessels identified with FITC–dextran and extravasation in the surrounding tissue. C, Image of the region outlined in (B) obtained using 2-photon laser scanning microscopy. An image stack was taken across the entire tissue section and axially projected as an average across all frames. Uptake of high-molecular-weight dextran–FITC is evident in both the large vessel as well as the smaller branch at the lower right of the image. Leakage of the dextran–FITC into the parenchyma can be seen in lower left quadrant of the image. D, A side projection of the highlighted region of the 2-photon laser scanning microscopy image stack shown in (C). The vessel cross-section shows a hollow vessel lumen. The projection is an average across 4 μm and spans the entire axial extent of the tissue section, ensuring that the fluorescence seen to the left of the vessel is caused by leakage, presumably from the imaged vessel.

wall. The vessel lumen was clear (Figure 2D), consistent with the effective washout of labeled plasma with transcardial perfusion fixation. This suggests that macromolecular dextran–FITC can lodge at high concentrations in ischemic endothelial cells and also escape from these vessels into surrounding parenchyma. Animals (n=6) were infused with high-molecular-weight dextran–FITC intravenously and then subjected to transient middle cerebral artery occlusion of 2 or 8 hours, followed by 30 minutes of reperfusion. Sections from the mid-parietal cortex were processed for optimal ultrastructural visualization as noted, and 3 blocks of tissue were selected based on the pattern of high-molecular-weight dextran–FITC labeling to include regions with high dextran distribution, low dextran distribution, and contralateral site (Figure 3). To image the ultrastructural deposition of bound fluorescein–dextran, the tissue was reacted with antifluorescein antibody and converted to diaminobenzidine, an electron-dense reaction product. Ischemic vessels that were labeled with diaminobenzidine were distinguished by electron-dense cytoplasmic labeling in constituent endothelial cells. These labeled endothelial cells were typically swollen (Figure 3C). Endothelial cells of vessels from low leakage ischemic areas or from the contralateral side were not obviously enlarged (Figure 3D, 3E). We used stereological analysis to quantify ultrastructural changes in tissues surrounding vascular disruption as labeled with high-molecular-weight dextran–FITC (Figure 4). Ipsilateral to the occlusion, the total areas of endothelial cells (including lumena) were slightly decreased compared to the opposite control side, consistent with edematous compression (data not shown), but the ratio of endothelial cell area to lumen was markedly increased in areas of high leakage, compared to areas of low leakage or contralateral side (Figure 4C; $P<0.001$; 1-way ANOVA; Tukey post hoc test). We demonstrated significant increases in the density of swollen mitochondria and astrocytes, and empty voids indicative of severe edema (Figure 4C). In regions of high leakage, the average area of astrocytic end-feet and structureless spaces were significantly larger—consistent with swelling as seen in cytotoxic edema—compared to areas with lower amounts of high-molecular-weight dextran–FITC signal, or corresponding subregions on the contralateral side ($P<0.001$; 1-way ANOVA; Tukey post hoc test). Greater numbers of swollen mitochondria were found in association with vascular labeling with high molecular weight dextran–FITC (Figure 4C; $P<0.001$; 1-way ANOVA; Tukey post hoc test).

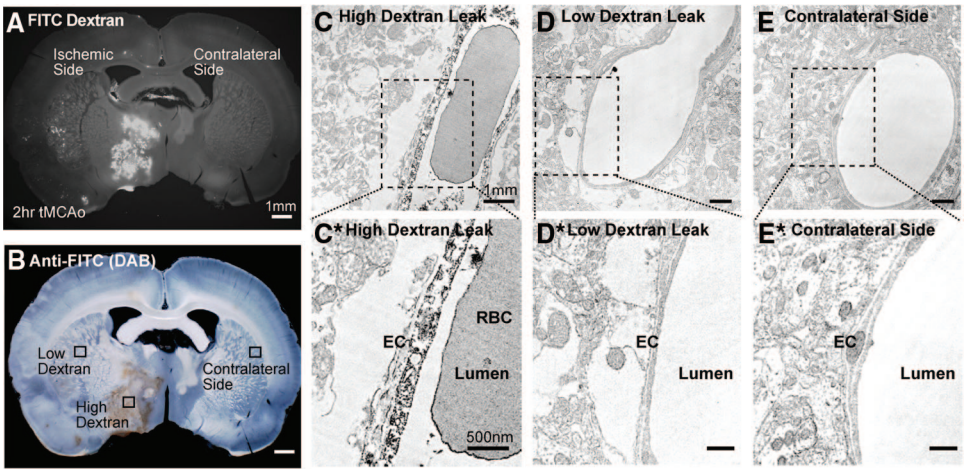

Figure 3. Ultrastructural localization of high-molecular-weight dextran–FITC. The localization of fluorescence (A) was confirmed using anti-FITC and a secondary reporter imaged with diaminobenzidine (B). Using FITC fluorescence on vibratome sections, we selected blocks from regions of high dextran accumulation, low dextran accumulation, and homologous sections from the contralateral sides. Ultrastructural examination at 5000× magnification revealed significant vascular labeling of the endothelial cells in regions of high-dextran fluorescence (C) and far less labeling in regions of low-dextran fluorescence (D) or the contralateral side (E). Higher-power views of the selected regions of interest are shown in C*, D*, and E*, respectively. C* demonstrates label contained in endothelial cells and some gross poration of the cell membrane.

Localization of Tissue Damage to Regions With Severe Vascular Disruption

We demonstrated tissue damage associated with areas of severe vascular disruption using multiple approaches. In 11 animals with variable durations of occlusion followed by reperfusion until 24 hours after onset of occlusion, the area of high-molecular-weight dextran–FITC leakage correlated well with the volume of tissue damage as labeled by 2,3,5-triphenyltetrazolium chloride staining (Figure 5; correlation coefficient $r=0.75$; $r^2=0.56$; $P<0.05$). Neuronal degeneration, labeled with Fluoro-Jade, was also observed in regions of high-molecular-weight dextran–FITC leakage in 10 animals (Figure 6; $r=0.86$; $r^2=0.75$; $P<0.05$). These findings together establish that high-molecular-weight dextran–FITC leakage serves to identify areas of severe vascular disruption and ischemic tissue injury.

BBB Leakage Areas Exceed Areas of Severe Vascular Disruption

To determine whether vascular disruption labeled with high-molecular-weight dextran–FITC merely served to identify areas of BBB leakage, which could be reversible, we compared the distribution of IgG leakage to vascular disruption in 20 animals (Figure 7). We found a significant dissociation between BBB leakage as labeled with IgG, compared to areas of severe vascular disruption, at multiple durations of middle cerebral artery occlusion (Figure 7; 1-way ANOVA; $P<0.001$; Tukey post hoc test). At all occlusion durations, the area of BBB leakage greatly exceeded the area of vascular disruption. The extent of BBB leakage reached a maximum by 4 hours of occlusion; but in contrast, the time course of severe vascular disruption was slower and showed greatest leakage at 8 hours, the longest duration we studied.

Discussion

Our data demonstrate that severe vascular disruption allows passage of high-molecular-weight dextran–FITC that is time-dependent and maximal in the brain regions made ischemic after occlusion of the middle cerebral artery (Figures 1, 2, 3).[12] With longer durations of ischemia, the high-molecular-weight dextran–FITC label accumulates with greater concentration in areas of basal lamina disruption, endothelial and astrocytic swelling, and eventually with total vascular poration (Figures 3, 4). Further, as the degree of vascular disruption increases, there is a corresponding increase in the extent of associated tissue damage (Figures 4, 5, 6). The label can be used to identify regions of brain undergoing severe vascular disruption as early as 1 hour after onset of ischemia (Figure 7). This suggests that brain regions suffering the most severe degree of ischemic injury after vascular occlusion can be labeled easily with a simple intravenous infusion of an inexpensive fluorescent maker. As shown in Figure 3, the presence of the marker can be used to select tissue that is undergoing significant vascular disruption and tissue damage for further detailed study. To our knowledge, this is the first simple marker of severe tissue injury that can be used easily and reproducibly as early as 1 hour after ischemia onset. We used high-molecular-weight dextran–FITC leakage to demonstrate a significant downregulation of the Aquaporin 4 receptor in regions of severe vascular disruption, further supporting the relationship between severe vascular disruption and tissue injury.[13]

The loss of BBB function in ischemic vasculature has been extensively studied and well-established with a variety of quantifiable tracers including isotopically labeled proteins and amino acids,[14–18] isotopically labeled sucrose,[19] fluorescent tracers,[20–22] and with MRI contrast agents.[23] Typically, quantification is made in terms of average vessel leakiness. The time course of increased leakage observed in the present study is consistent with that observed by previous spectrophotometric methods.[21] Additionally, the gross regional specificity of our results are consistent with the low-resolution spatial patterns of BBB observed with MRI, which demon-

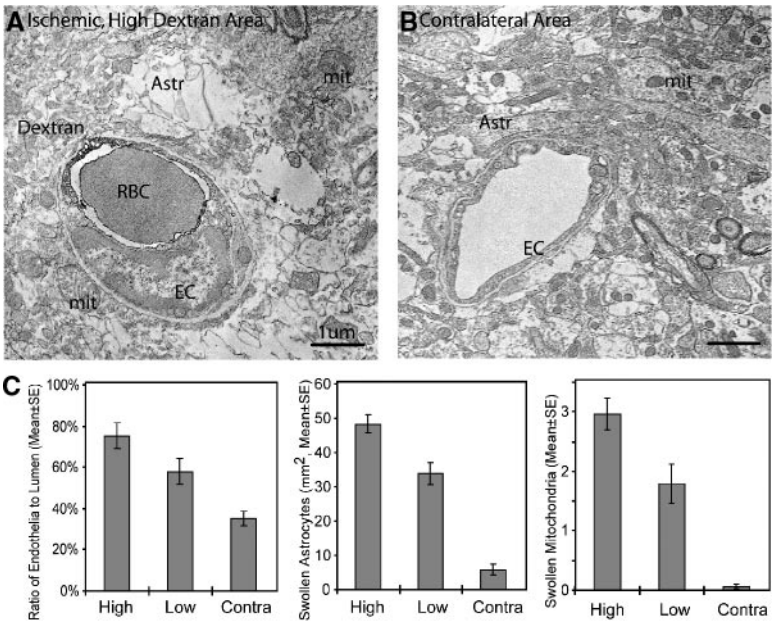

Figure 4. Vascular disruption and cytotoxic edema results in areas of high-molecular-weight dextran leakage. Using tissue blocks from areas of high- or low-dextran accumulation and the homologous contralateral sections (n=6) selected as in Figure 2, we examined serial 50-nm-thick sections. Using an unbiased stereological counting grid, we estimated the areas of endothelial cells and astrocytes, as well as the areas of "featureless void" that likely represent water accumulation. We also identified swollen mitochondria by visual inspection, defined as mitochondria appearing to be twice the size or larger of mitochondria seen on the contralateral region. Note that in areas of significant accumulation of fluorescent high-molecular-weight dextran (A) there are extremely swollen astrocytes (Astr) and mitochondria (mit). Also, the cytoplasm of the endothelial cells is greatly expanded, compared to the contralateral side (B) or the low-dextran region (not illustrated). The averaged results from 138 sections are summarized with standard errors in (C). Because of the opposite effects of cytoplasmic swelling and luminal compression caused by edema, the total endothelial areas (including lumen) are approximately comparable between areas of high and low dextran accumulation, and both are somewhat less than the contralateral side (data not shown). The ratio of endothelial cell area to lumen area (C, left panel) clearly demonstrates significant cytotoxic edema and luminal compression in areas of high leakage, compared to areas of lower leakage and the contralateral side (ANOVA $P<0.001$; Tukey test for posthoc comparisons). The accumulation of increasing quantities of high-molecular-weight dextran–FITC was significantly associated with astrocyte swelling (C, middle panel; ANOVA $P<0.0001$; using Tukey test for post hoc comparisons; all pair-wise comparisons were significant; $P<0.01$). Similarly, the number of swollen mitochondria per field increased with increasing dextran accumulation (C, right panel; ANOVA $P<0.0001$; using Tukey test for post hoc comparisons; all pair-wise comparisons were significant; $P<0.01$).

strate early contrast enhancement (2.5 hours of occlusion) in the ventral striatum of the adult rat.[23]

The mechanism of high-molecular-weight dextran leakage is not established unequivocally by our data, although inspection of the ultrastructure (Figures 3, 4) suggest that both increased transcytosis and gross cellular poration are involved. Using similar approaches, the leakage of small-molecular-weight albumin was shown to precede and show more extensive staining than the leakage of large-molecular-weight dextran.[12] Considerable literature addresses the leakage of smaller-molecular-weight molecules via loosening of the tight junctions between endothelial cells, but there is debate over the roles of transcytosis and transmembrane poration.[24–26] Our data do not address the role of tight junction loosening in the mechanism of higher-molecular-weight dextran leakage, but the time course and spatial distribution of vessel ischemia, as demonstrated by high-molecular-weight dextran–FITC uptake, is consonant with the molecular events that underlie BBB breakdown after experimental large vessel occlusion.[27] Proteolytic breakdown of BBB structural molecules[19] is an early event that occurs within 1 to 2 hours after an ischemic insult.[19,27–31] Immunocytochemical imaging studies of molecular changes in other neural compartments illustrate that they also occur in a spatially heterogeneous fashion,[32,33] forming "islands" of altered protein expression that have been purported to represent small infarctions in both the ischemic striatum and cortex. The temporal and spatial development of severe vascular disruption (Figure 1) appears to coincide with these well-documented molecular events and whereas our data do not allow us to confirm a mechanistic link, the technique we present here will greatly facilitate such mechanistic investigations in the future.

Our study comes with some limitations. High-molecular-weight dextran–FITC is detected directly, without amplification; other markers, including the low-molecular-weight marker IgG, are detected after antibody labeling, which could amplify the signal. The degree of difference between IgG leakage vs high-molecular-weight dextran leakage (Figure 7) likely exceeds the possible amplification step, but such an effect cannot be excluded by our data. Tissue injury markers such as 2,3,5-triphenyltetrazolium chloride exclusion and Fluoro-Jade uptake, although standard in the field, are not synonymous with cell death, nor do they differentiate between necrotic and apoptotic cell death mechanisms. We cannot assert that the severe vascular disruption identified with high-molecular-weight dextran–FITC marks regions of brain undergoing

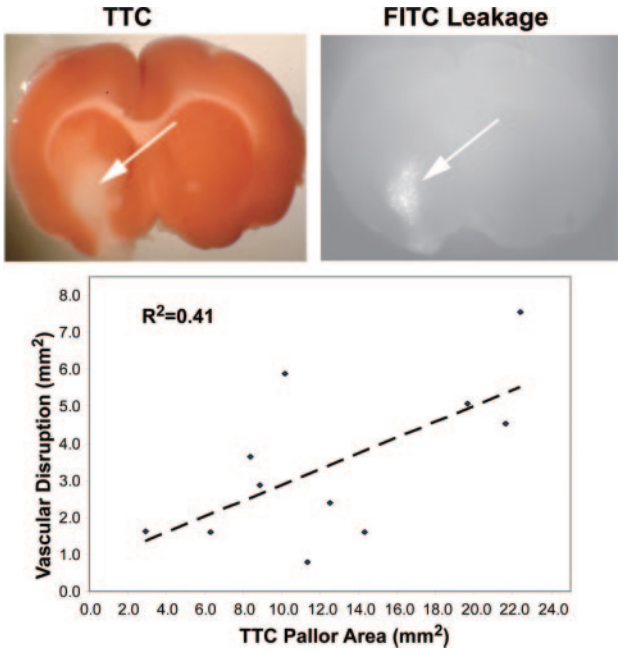

Figure 5. Accumulation of high-molecular-weight dextran–FITC in areas of significant tissue injury. Vascular disruption was compared to tissue injury after varying durations of ischemia (2 hours, n=4; 3 hours, n=5; 4 hours, n=1; each time point marked with a different symbol). High-molecular-weight dextran–FITC was administered before middle cerebral artery occlusion, and again just before euthanization. After 24 hours of reperfusion and euthanization, brains were immediately processed in 2,3,5-triphenyltetrazolium chloride to visualize the region of cellular injury and photographed. The sections were then fixed, imaged, and photographed under fluorescence optics. Scrambled identifiers were used to label the 2,3,5-triphenyltetrazolium chloride and the fluorescent images. Using calibrated planimetry, one examiner traced the areas of 2,3,5-triphenyltetrazolium chloride pallor and then traced the area of fluorescence in a masked fashion. After unblinding, the measurements were linked and compared. The scatterplot shows 10 data pairs. There was a significant correlation between 2,3,5-triphenyltetrazolium chloride pallor and the accumulation of high-molecular-weight dextran–FTIC (Pearson r=0.75; P=0.05; R^2=0.56).

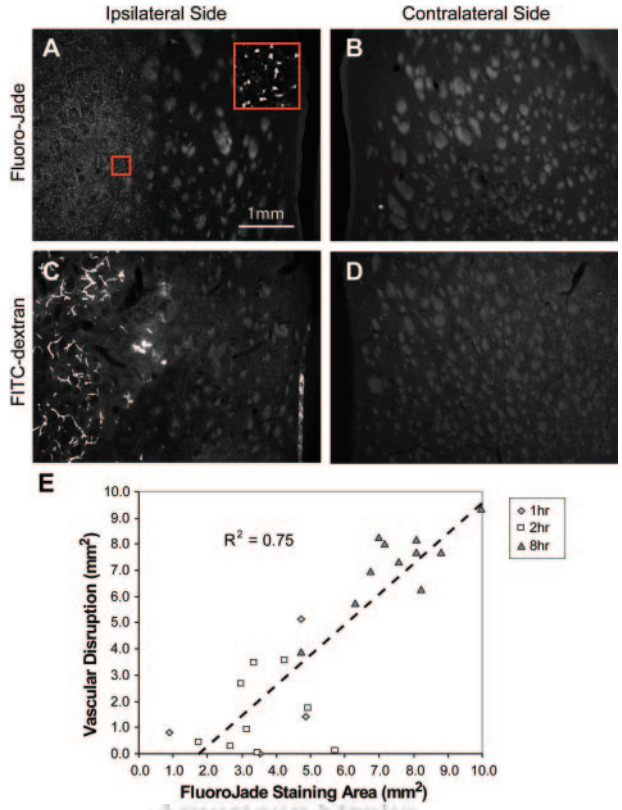

Figure 6. Significant cytopathology results in areas of accumulation of high-molecular-weight dextran–FITC. In the hemisphere ipsilateral (A) and contralateral (B) to the middle cerebral artery occlusion, we compared the extent of cytotoxic injury (using the cell-injury marker Fluoro-Jade) to the area of accumulation of high-molecular-weight dextran–FITC in the ipsilateral (C) and contralateral (D) hemispheres. On high-power examination (inset in A), the Fluoro- Jade is clearly localized to cell bodies that resemble neurons, but cell-specific markers were not used to differentiate neurons from astrocytes. As in Figure 5, a single examiner traced the areas of Fluoro-Jade uptake and, in a masked fashion, independently traced the areas of dextran accumulation (n=10 animals, 2 to 3 sections per animal, ischemia durations of 1 hour, n=3; 2 hours, n=3; 8 hours, n=4; each time point marked with a different symbol). After unblinding and linking the measurements, there was a highly significant relationship between the leakage marker and cytopathology (Pearson r=0.86; P<0.05; R^2=0.75).

irreversible ischemic damage that will inevitably become infarct, although it is difficult to believe that areas showing such severe injury (Figures 3, 4) could recover. Further studies are needed to: (1) show that such marked areas do not possess the ability to recover; (2) identify the mechanisms of severe vascular disruption; and (3) determine if protective agents that inhibit severe vascular disruption also block the associated tissue injury. Another limitation is the relatively biased sampling strategy we used for selecting sections for ultrastructure. A purely random sampling strategy would be unbiased, and might allow one to determine whether evidence of severe vascular disruption is found only in areas of greatest high-molecular-weight dextran leakage. However, such a sampling strategy is difficult for cost and time reasons. To overcome this selection bias, all sections were reviewed in semi-blinded fashion. In other words, in double-labeling experiments, images were taken from all sections using one label, then scrambled, and all sections were reimaged using the second label. Similarly, in the planimetry and point-counting assessments, the investigator examined all sections of one label, and then reviewed all the sections using the other label after scrambling de-identified sections. With these limitations in mind, the argument that high-molecular-weight dextran leakage occurs in areas of vascular disruption and tissue injury is supported by the fact that we used multiple, complimentary imaging techniques, all of which clearly show the same, highly statistically significant relationship. We specifically hypothesized that vascular disruption and tissue injury would occur in areas of greater dextran leakage, and our data support this hypothesis directly (Figures 5, 6).

We have demonstrated that a simple, inexpensive, intravenous marker—high-molecular-weight dextran–FITC—reproducibly labels brain regions undergoing severe vascular disruption and associated tissue injury before the development of obvious infarction. Labeling is greatest in the regions

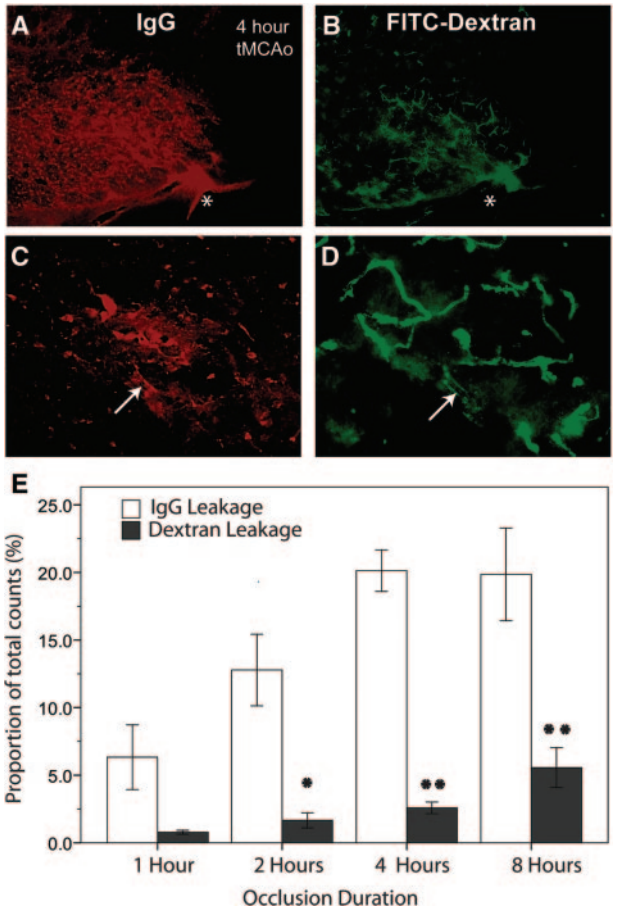

Figure 7. Vascular disruption occurs within a larger region of BBB leakage. After 1 hour (n=4), 2 hours (n=5), 4 hours (n=5), or 8 hours (n=6), middle cerebral artery occlusion followed by 30 minutes of reperfusion, we measured the quantities of IgG and high-molecular-weight dextran in the images, using double-labeled fluorescence microscopy. Fluorescence was quantified with laser scanning microscopy, and the counts in each channel normalized to the total counts present in the section. A, In a representative example, IgG leakage (Cy5 channel) appeared to be more homogenous and not confined to vessels. B, The same section was imaged using the FITC channel, showing a much more heterogeneous appearance and localization to the vessels. The asterisk (*) is placed in the ventricle to demonstrate image registration. Higher-magnification views of IgG leakage (C) and high-molecular-weight dextran leakage (D) confirm the vascular localization of the dextran; the arrows point to a vessel with significant retention of IgG and, in a more heterogeneous pattern, dextran–FITC. The average proportions with standard errors are shown for each occlusion duration (E). The proportion of counts showing the IgG leakage (Cy5) exceeded the proportion showing dextran leakage (FITC) in all sections studied at all time points (independent samples *t* tests, $P<0.05$ after Bonferroni correction). Leakage of IgG appeared to reach a maximum by 4 hours of middle cerebral artery occlusion, but dextran leakage appeared to increase at each time point up to 8 hours (1- way ANOVA for time, $P<0.001$ for dextran).

of brain known to suffer the greatest degree of ischemia after middle cerebral artery occlusion and increasing durations of ischemia cause greater amounts of labeling. This marker will allow for further studies of the mechanisms of vascular injury, and the relationships between vascular, glial, and neuronal cell injury mechanisms, by providing a simple way to identify severely damaged tissue as early as 1 hour after ischemia onset.

Acknowledgments

The authors thank Rodolfo Figueroa for fabricating occluding filaments, Kai Yang for assisting in fluorescence quantification, Judy Norberg for performing the laser scanning cytometry, Dr Maryann Martone for helpful suggestions in ultrastructural imaging, and Drs Donald Pizzo and the late Leon Thal for use of their photomicroscope. B.C. thanks the HHMI-NIBIB Interfaces Training Program at UCSD.

Sources of Funding

This work was funded by the Veteran's Affairs Medical Research Department (P.D.L), by the National Institute of Health grants NS/043300, and NS/052565 (P.D.L.), NS/041096, and EB\003832 (D.K.).

Disclosure

None.

References

1. Hawkins BT, Davis TP. The blood-brain barrier/neurovascular unit in health and disease. *Pharmacol Rev*. 2005;57:173–185.
2. Latour LL, Kang DW, Ezzeddine MA, Chalela JA, Warach S. Early blood-brain barrier disruption in human focal brain ischemia. *Ann Neurol*. 2004;56:468.
3. Lo EH, Dalkara T, Moskowitz MA. Mechanisms, challenges and opportunities in stroke. *Nat Rev Neurosci*. 2003;4:399–415.
4. Figueroa BE, Keep RF, Betz AL, Hoff JT. Plasminogen activators potentiate thrombin-induced brain injury. *Stroke*. 1998;29:1202.
5. Jackson-Friedman C, Lyden PD, Nunez S, Jin A, Zweifler R. High dose baclofen is neuroprotective but also causes intracerebral hemorrhage: A quantal bioassay study using the intraluminal suture occlusion method. *Exp Neurol*. 1997;147:346.
6. Bederson JB, Pitts LH, Tsuji M, Nishimura MC, Davis RL, Bartkowski H. Rat middle cerebral-artery occlusion - evaluation of the model and development of a neurologic examination. *Stroke*. 1986;17:472.
7. Longa EZ, Weinstein PR, Carlson S, Cummins R. Reversible middle cerebral artery occlusion without craniectomy in rats. *Stroke*. 1989; 20:84.
8. Tsai PS, Friedman B, Ifarraguerri AI, Thompson BD, Lev-Ram V, Schaffer CB, Xiong Q, Tsien RY, Squier JA, Kleinfeld D. All-optical histology using ultrashort laser pulses. *Neuron*. 2003;39:27–41.
9. Nguyen QT, Tsai PS, Kleinfeld D. Mpscope: A versatile software suite for multiphoton microscopy. *J Neurosci Methods*. 2006;156:351–359.
10. Weibel ER. *Stereological methods: Practical methods for biological morphometry*. San Diego: Academic Press; 1989:volume 1.
11. Thorball N. Fitc-dextran tracers in microcirculatory and permeability studies using combined fluorescence stereo microscopy, fluorescence light microscopy, and electron microscopy. *Histochemistry*. 1981;71: 209–233.
12. Nagaraja TN, Keenan KA, Fenstermacher JD, Knight RA. Acute leakage patterns of fluorescent plasma flow markers after transient focal cerebral ischemia suggest large openings in blood-brain barrier. *Microcirculation*. 2008;15:1–14.
13. Friedman B, Schachtrup C, Tsai PS, Shih AY, Akassoglou K, Kleinfeld D, Lyden PD. Acute vascular disruption and aquaporin 4 loss after stroke. *Stroke*. 2009;40:2182–2190.
14. Brightman MW, Klatzo I, Olsson Y, Reese TS. The blood-brain barrier to proteins under normal and pathological conditions. *J Neurol Sci*. 1970; 10:215–239.
15. Yang GY, Betz AL. Reperfusion-induced injury to the blood-brain barrier after middle cerebral artery occlusion in rats. *Stroke*. 1994;25:1658.
16. Ennis SR, Keep RF, Schielke GP, Betz AL. Decrease in perfusion of cerebral capillaries during incomplete ischemia and reperfusion. *J Cereb Blood Flow Metab*. 1990;10:213–220.
17. Sage JI, Van Uitert RL, Duffy TE. Early changes in blood brain barrier permeability to small molecules after transient cerebral ischemia. *Stroke*. 1984;15:46–50.
18. Hossmann KA, Olsson Y. Influence of ischemia on the passage of protein tracers across capillaries in certain blood-brain barrier injuries. *Acta Neuropathol*. 1971;18:113–122.

19. Rosenberg GA, Estrada E, Dencoff JE. Matrix metalloproteinases and TIMPs are associated with blood-brain barrier opening after reperfusion in rat brain. *Stroke*. 1998;29:2189.
20. Steinwall O, Klatzo I. Selective vulnerability of the blood-brain barrier in chemically induced lesions. *J Neuropathol Exp Neurol*. 1966;25: 542–559.
21. Belayev L, Busto R, Zhao W, Ginsberg MD. Quantitative evaluation of blood-brain barrier permeability following middle cerebral artery occlusion in rats. *Brain Res*. 1996;739:88.
22. Dawson DA, Ruetzler CA, Hallenbeck JM. Temporal impairment of microcirculatory perfusion following focal cerebral ischemia in the spontaneously hypertensive rat. *Brain Res*. 1997;749:200–208.
23. Neumann-Haefelin T, Kastrup A, de Crespigny A, Yenari MA, Ringer T, Sun GH, Moseley ME. Serial mri after transient focal cerebral ischemia in rats. *Stroke*. 2000;31:1965.
24. Huber JD, Egleton RD, Davis TP. Molecular physiology and pathophysiology of tight junctions in the blood-brain barrier. *Trends Neurosci*. 2001;24:719.
25. Cipolla MJ, Crete R, Vitullo L, Rix RD. Transcellular transport as a mechanism of blood- brain barrier disruption during stroke. *Front Biosci*. 2004;9:777–785.
26. Lossinsky AS, Shivers RR. Structural pathways for macromolecular and cellular transport across the blood-brain barrier during inflammatory conditions. *Review Histol Histopathol*. 2004;19:535–564.
27. Hamann GF, Okada Y, Fitridge R, del Zoppo GJ. Microvascular basal lamina antigens disappear during cerebral ischemia and reperfusion. *Stroke*. 1995;26:2120–2126.
28. Maier CM, Hsieh L, Yu F, Bracci P, Chan PH. Matrix metalloproteinase-9 and myeloperoxidase expression: Quantitative analysis by antigen immunohistochemistry in a model of transient focal cerebral ischemia. *Stroke*. 2004;35:1169–1174.
29. Asahi M, Wang X, Mori T, Sumii T, Jung JC, Moskowitz MA, Fini ME, Lo EH. Effects of matrix metalloproteinase-9 gene knock-out on the proteolysis of blood-brain barrier and white matter components after cerebral ischemia. *J Neurosci*. 2001;21:7724–7732.
30. Heo JH, Lucero J, Abumiya T, Koziol JA, Copeland BR, del Zoppo GJ. Matrix metalloproteinases increase very early during experimental focal cerebral ischemia. *J Cereb Blood Flow Metab*. 1999;19:624.
31. Hosomi N, Lucero J, Heo JH, Koziol JA, Copeland BR, del Zoppo GJ. Rapid differential endogenous plasminogen activator expression after acute middle cerebral artery occlusion. *Stroke*. 2001;32:1341–1348.
32. Tagaya M, Haring HP, Stuiver I, Wagner S, Abumiya T, Lucero J, Lee P, Copeland BR, Seiffert D, del Zoppo GJ. Rapid loss of microvascular integrin expression during focal brain ischemia reflects neuron injury. *J Cereb Blood Flow Metab*. 2001;21:835.
33. Sharp FR, Lu A, Tang Y, Millhorn DE. Multiple molecular penumbras after focal cerebral ischemia. *J Cereb Blood Flow Metab*. 2000;20:1011.